

Preparation and microwave absorbing properties of graphene oxides/ferrite composites

Kun Liang¹ · Xiao-Jing Qiao¹ · Zhi-Gang Sun² · Xiao-Dang Guo³ · Long Wei¹ · Yang Qu¹

Received: 26 April 2016 / Accepted: 22 May 2017 / Published online: 26 May 2017
© Springer-Verlag Berlin Heidelberg 2017

Abstract The graphene oxides (GO) and the graphene-based composites have been synthesized successfully by Hummer method and Hydrothermal-calcination process, respectively. The effects of solvent (water, ethylene glycol, glycerol and glycol–glycerol), the consumption of graphite oxides (GO = 0.1, 0.5, 1.0, 2.0 wt%) on the crystallization, morphology and performance of the target samples have been investigated. The obtained samples have been characterized by FTIR, XRD, SEM and HRTEM. The precursors obtained through hydrothermal process are composed of 80 nm ferromagnetic polyhedral particles and the uniformly distributed covering GO layers. After calcination, the 200 nm ferromagnetic nanoparticles can be achieved on the surface of graphene films. The results indicate that the optimized samples can be obtained at

GO = 0.1 wt% under water system. Also, the electromagnetic properties and microwave absorbing performance have been measured by VNA. The addition of GO is conducive to improve the absorbing property of ferrites by shifting the reflectivity peak into lower frequency range and sharpening the maximum value. At GO = 0.1%, the maximum RL peaks can reach -17.15 dB at 3.3 GHz, with the bandwidth below -10 dB ranging from 2.8 to 3.8 GHz under 3 mm thickness. For GO = 1.0 wt%, twin peaks appear at 4.3 and 15.6 GHz of 3.5 mm thickness, and the bandwidth below -10 dB reaches 2.6 GHz (10.3–12.9 GHz) at 1.5 mm thickness.

1 Introduction

With the development of the modern military reconnaissance technology, the interest in designing and preparing stealth absorbers has been aroused widely to be a kernel countermeasure response to military threat [1–4]. Shape and structure design and absorbing materials selection must be taken into consideration when the absorbers are being designed [5–7].

Graphene is a 2D honeycomb-like sheet of carbon with a number of unique physical properties, such as the unique crystal structure and electronic properties, good thermal conductivity, high mechanical properties and excellent electrical transport properties [8, 9]. In recent years, graphene has attracted more and more attention. It is used not only in validating important theoretical physics [10], but also in providing a broad application prospects for industrial production, such as wave adsorbing materials [11], sensors [12], capacitors [13], and so on [14, 15].

Due to the unique performance, such as small density, large specific surface area, and excellent dielectric

✉ Xiao-Jing Qiao
qxjbit84@163.com

Kun Liang
lk.mr@hotmail.com

Zhi-Gang Sun
710784793@qq.com

Xiao-Dang Guo
375408644@qq.com

Long Wei
814890872@qq.com

Yang Qu
qy2120150225@163.com

¹ School of Mechatronic Engineering, Beijing Institute of Technology, Beijing 0086100081, China

² Institute 206, Second Academy of China Aerospace Science and Industry Corporation, Beijing 0086100854, China

³ Beijing Electro-Mechanical Engineering Institute, Beijing 0086100074, China

constant [16, 17], graphene makes it easier for polarization relaxation from outer electrons under the excitation of electromagnetic field, which indicates that the graphene possesses good application prospect in the field of microwave absorbing. However, because of the weak magnetic loss property, the absorbers composed of single graphene cannot meet the demands of the small thickness, light weight, wide frequency and high efficiency. The composite materials, composed by graphene, metal nanoparticles and organic small molecules, etc. can make up the weakness of single components to improve the microwave absorbing performance [18, 19]. Nowadays, researchers focus their attention on the combination of graphene and magnetic materials, such as Pd [20], Fe₃O₄ [21], CoFe₂O₄ [22], NiFe₂O₄@SiO₂ [23], Ag/MnFe₂O₄ [24], and so on [25, 26]. However, there are only a few literatures that can be found in the study of the Graphene oxides/Ferrite composites to be the perfect microwave absorbers, especially for the lower frequency range [27].

Here, in this paper, in order to introduce functional groups, such as hydroxyl, carboxyl, carbonyl and epoxy groups, into the interlayer of graphene, graphene oxides (GO) have been prepared successfully by Hummers' chemical oxidation process, firstly [28, 29]. Then, the GO have been ultrasonic dispersed, mixed with ferric salts and reduced through solvothermal synthesis process in an atmosphere composed by hydrazine hydrate and sodium borohydride to prepare the precursors [30]. Finally, GO/Ferrite composites have been prepared by roasting the precursors at high temperature.

2 Experimental methods

The chemical reagents include ferrous chloride (FeCl₂·4H₂O), cobalt chloride hexahydrate (CoCl₂·6H₂O), natural flake graphite (99.8%, 200 mesh), sulfuric acid (H₂SO₄, 98.0%), potassium permanganate (KMnO₄, 99.0%), sodium nitrate (NaNO₃, 99.0%), hydrogen peroxide (H₂O₂, 60%) and hydrochloric acid (HCl, 35.8%), ethylene glycol (C₂H₆O₂, 99.0%), glycerol (C₃H₈O₃, 99.0%), glucose (C₆H₁₂O₆, 99.0%), urea (CO(NH₂)₂, 99.0%), and nitrogen (N₂, 99.99%). All the reagents except the nitrogen are analytical pure reagents, purchased from Sinopharm Chemical Reagent Co. Ltd. The equipment includes the PTFE hydrothermal kettle, bench centrifuge (Beijing Force Centrifuge Co. Ltd.), SGM28 tube furnace (Luoyang Sigma Instrument Manufacturing Co Ltd.), quartz tube (99.99%, SiO₂, Alpha Quartz Products Co. Ltd.) and corundum tube (99.99%, Al₂O₃, Zhong Bote Co. Ltd.).

The GO have been synthesized by the Hummers method [31]. 3.0 g graphene and 1.5 g NaNO₃ are put in a three-necked bottle. 69 ml concentrated sulfuric acid is added

into the system. Under magnetic stirring, 9 g KMnO₄ is added into the system slowly below 20 °C and the temperature is kept at 35 °C for 30 min. Then, 138 mL deionized water are added into the system and kept at 98 °C for 15 min. After cooling to room temperature, 420 mL deionized water and 30 ml H₂O₂ (30 vol%) are added. Then, the target GO are being prepared after being purified in water and ethanol and dried at 60 °C for 12 h.

To synthesize the GO/Ferrites composites, 0.1 wt% GO are put in 65 ml solvent under 30 min ultrasonic dispersion firstly. And then 20 mmol FeCl₂·4H₂O and 10 mmol CoCl₂·6 H₂O are added into the system and kept ultrasonic-dispersing for 40 min. And 3 ml hydrazine hydrate, 3 g urea is added into PTFE hydrothermal kettle and reacted for 14 h under 160 °C. After washed with distilled water and ethanol and centrifugal separation several times to pH 7, the GO/Ferrite precursors have been prepared. Finally, the target GO/Ferromagnetic composites can be prepared by putting the precursors into tube furnace under 0.1 MPa at N₂ atmosphere and reduced at 650 °C for 3 h by activated carbon. Different factors of the solvent [water, ethylene glycol, glycerol and glycol-glycerol (5.5:1)], the consumption of graphite oxide (GO = 0.1, 0.5, 1.0, 2.0 wt%) on the morphology and performance of the target samples have been investigated by parallel experiments.

The sample components and crystallization degree have been confirmed by X-Ray Diffraction-XRD (ULTIMATV RIGAKU, Cu K_α, λ₀ = 1.54056 Å, scanning rate at 0.02 °/s, scanning range 10°–80°), Fourier Transforms Infrared Spectroscopy-FTIR (Bruker Equinox 55, KBr). The microstructure and crystallization of the precursors and target samples have been evaluated by the Scanning Electron Microscope-SEM (Hitachi S4700) and the High Resolution Transmission Electron Microscopy-HRTEM (JEM2100F, 200 kV). Electromagnetic parameters were analyzed with a Vector Network Analyzer-VNA (Agilent 8722ES), and the specimens were prepared by uniformly mixing 60 wt% samples with 40 wt% paraffin. The complex permittivity and the complex permeability were measured by the T/R coaxial line method (input power level –5.0 dBm). The reflection loss (RL) can be calculated from the aforementioned parameters.

3 Results and discussion

3.1 FTIR analysis

The FTIR patterns of graphene and GO are depicted in Fig. 1. The characteristic peaks at 3400 and 1620 cm⁻¹ belong to the stretching vibration of O–H and C=C bonds of graphene. After being oxidized, some characteristic peaks appear, such as the stretching vibration of C=O

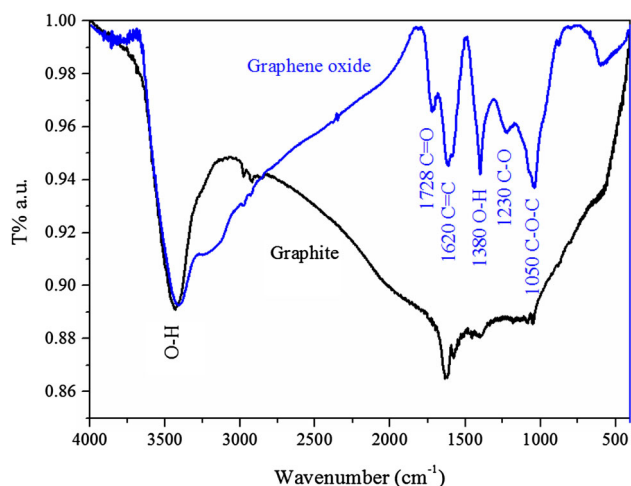


Fig. 1 The FTIR patterns of graphene and GO

bonds at 1728 cm^{-1} and characteristic tips of C–O–C bonds at 1230 and 1050 cm^{-1} , which indicates the introduction of kinds of functional groups into the graphene layers.

3.2 XRD analysis

Figure 2 shows the XRD patterns of graphene, GO and GO/Ferrite composites under corresponding conditions (scanning rate $0.02\text{ }^\circ\text{ s}^{-1}$, range 10° – 80°). The peaks at 26.0° are the characterization peaks of the Graphite 2H (PDF # No. 08-0415), consistent with that of the (111) crystal plane. From the XRD pattern of GO, it can be seen that the peaks at 26.0° of graphene disappear, with the characteristic tips at 12.1° of GO existed, which reveals the oxidation of graphene. Corresponding with the (002) crystal plane, the lattice spacing of the samples is about 0.735 nm , according to the Scherrer formula as follows:

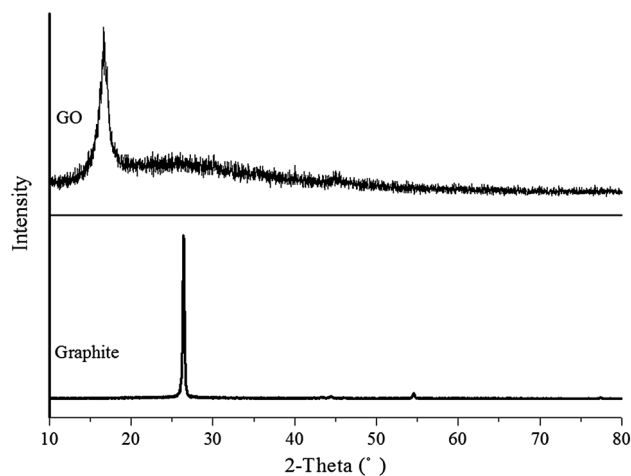


Fig. 2 The XRD patterns of the graphene and the GO

$$D = K\lambda/\beta\cos\theta \quad (1)$$

where K is the Scherrer constant, about 0.89; D is the grain size (nm); and β is the FWHM of the characterization peak.

The XRD patterns of the target materials in different solvents at GO = 0.1% have been depicted in Fig. 3. With water as solvent, the samples of hydrothermal process are mainly CoFe_2O_4 , with the characteristic peaks narrow and sharp, reflecting a better crystal growing process. In ethylene glycol, a poor crystallization of CoFe_2O_4 appears, which is inferior to the product in water system. When the glycerol or glycol–glycerol (5.5:1) is selected as solvent, the main phase of the precursors is FeCO_3 and CoCO_3 . After $650\text{ }^\circ\text{C}$ calcination, with water and glycol as solvent, parts of the ferrite are reduced to Co and FeCo metal alloys. While, in glycerol or glycol–glycerol (5.5:1) system, FeCO_3 is decomposed into more CoFe_2O_4 and less FeCo alloys.

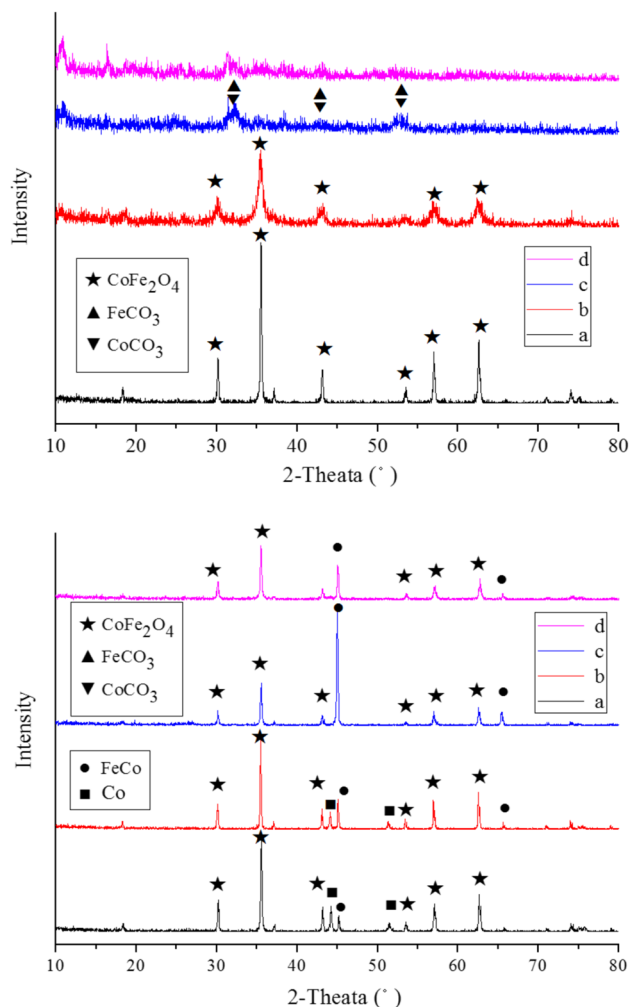


Fig. 3 The XRD patterns of the precursors and the target samples at different solvents (a water, b ethylene glycol, c glycerol and glycol–glycerol (5.5:1), d glycerol)

In Fig. 3, it also shows that the samples after calcination in ethylene glycol and glycerol are mainly FeCo alloys, with no GO existed, which indicates the thorough reduction process of the samples. While, the bread characteristic tips of the graphene appear at about 24° [32], which is in accordance with the XRD results in the literature [33]. After combination, only the characteristic peaks of Ferrites appear with no graphene peaks, which may be because the CoFe_2O_4 particles destroy the ordered structure of graphene.

Similarly, the effect of the consumption of GO on the crystallization of the samples has been characterized in Fig. 4. Comparatively, on condition of 0.5 or 1.0 wt% GO, the wide and weak characteristic peak at 26.3° appears, as well as the characteristic peaks of the ferrites, which indicates the preparation of CoFe_2O_4 and FeCO_3 [34], while the FeCo alloy can be obtained at $\text{GO} = 1.0$, and 2.0 wt% of GO corresponding to the Co phase. The results indicate that along with the increase of GO, the GO/Ferrite

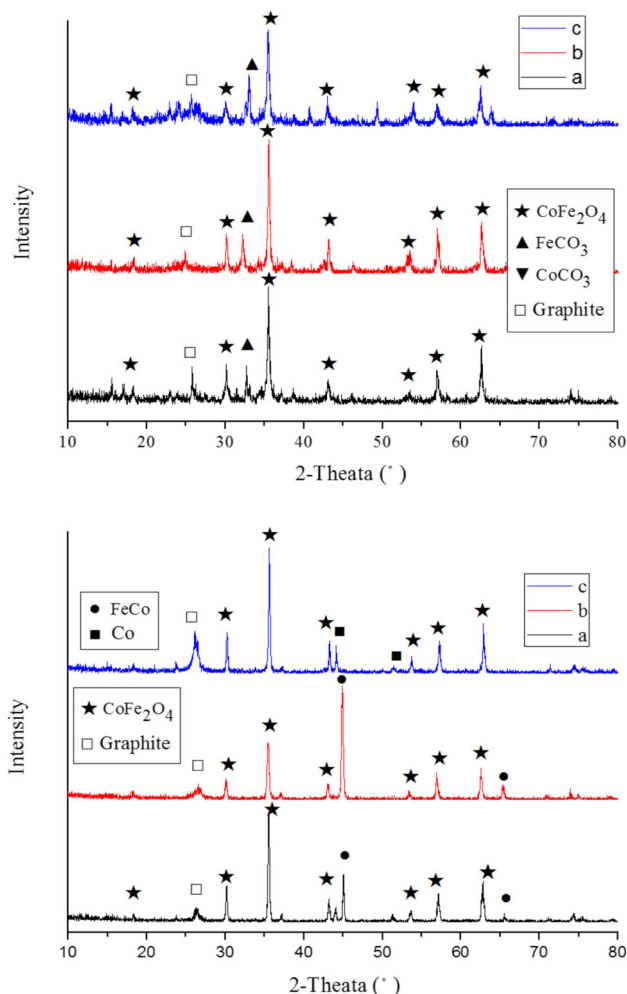


Fig. 4 The XRD spectrum of the precursors and the target samples under different mass of GO (a 0.5 wt%; b 1.0 wt%; c 2.0 wt%)

composites have been prepared all the more easily, while the ferrites will be reduced greatly if the graphene is increased blindly.

3.3 SEM and HRTEM analysis

Figure 5 shows the SEM and TEM images of the GO samples by Hummers method. After acidification process, lots of 300 nm thickness multilayer GO have been synthesized. From the HRTEM graphs of Fig. 5b, the evenly dispersed curled single GO layer has been found after 30 min dispersion in ethanol. That is because the dangling bonds of GO may lead to the unstable structure for the large surface area ratio and high surface energy, and only the curled structure can keep the system stable [35].

Figure 6 shows the SEM patterns of the samples in different solvents. In water, as it is shown in Fig. 6a, b, the samples with polyhedron structure are dispersed on the surface of the graphene evenly, with the thickness increased to about 300 nm and diameter about 80 nm. With ethylene glycol as solvent, the 100 nm roughly dispersed particles appear, as it is depicted in Fig. 6c, d, while, after 20 ml glycerol added into the system, a state of porous softy composites existed in Fig. 6e, f. With glycerol as solvent, the absorption properties of the magnetic materials become weaker than those of others, with the unusual morphology and unevenly dispersion. From the results, it can be deduced that the dispersion and morphology of the samples are largely affected by the viscosity of the solvent, and the formation of the polyhedron structure is promoted by low viscosity system. However, for the stronger viscosity system, such as glycerol, it leads to the synthesis of spherical particles, and the ferrites grow along the special planes for the inducement of the hydroxyl radicals and result in the formation of nanowires. While it is not the same with the condition of glycerol system, that is because the stronger viscosity is unfavorable to the dispersion and adsorption of the Fe^{2+} and iron transition and leads to the uneven dispersion and unusual structure, as it is presented in Fig. 6g, h.

Figure 7 shows the SEM pattern of the target GO/Ferrite composites in different solvents. As it is presented in Fig. 7a, b, the nanometer Ferrites are absorbed on the graphene surface, with the diameter increased to 300 nm. That is because the samples can be sintered at higher temperature, which makes the Ferrites attached with graphene easily to be large stable particles. The SEM patterns of the target samples in ethylene glycol are shown in Fig. 7c, d. It can be seen that the 300 nm ferrite particles are absorbed on both sides of the graphene sheets and wrapped by filamentous polymers, which may result from the decomposition of ethylene glycol. With ethylene glycol and glycerol as solvent, the target samples are mainly

Fig. 5 The SEM and HRTEM images of the GO samples

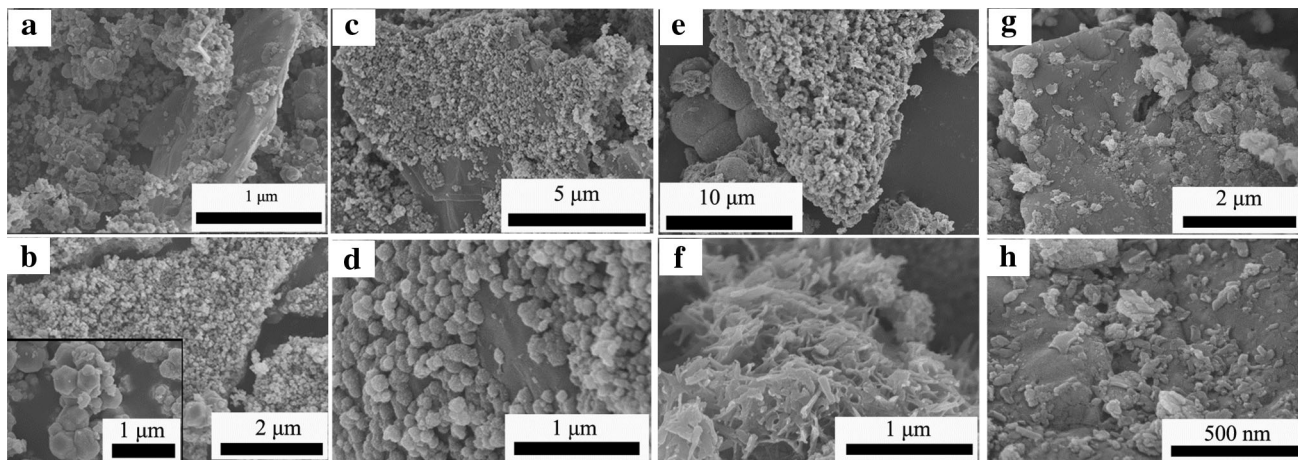
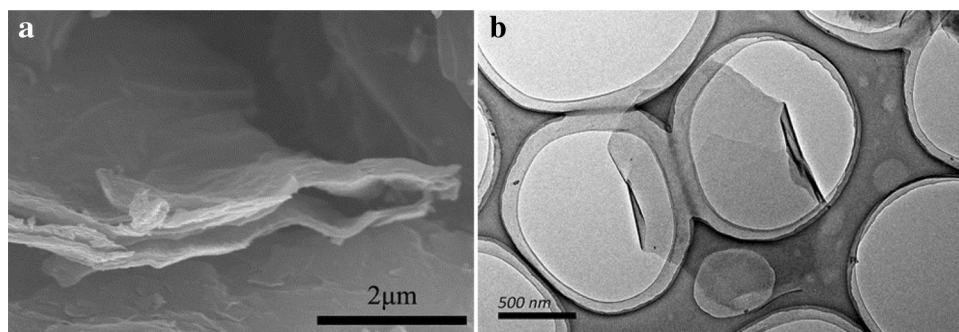


Fig. 6 The SEM patterns of the precursors in different solvents at GO = 0.1% (a, b water; c, d ethylene glycol; e, f ethylene glycol and glycerol; g, h glycerol)

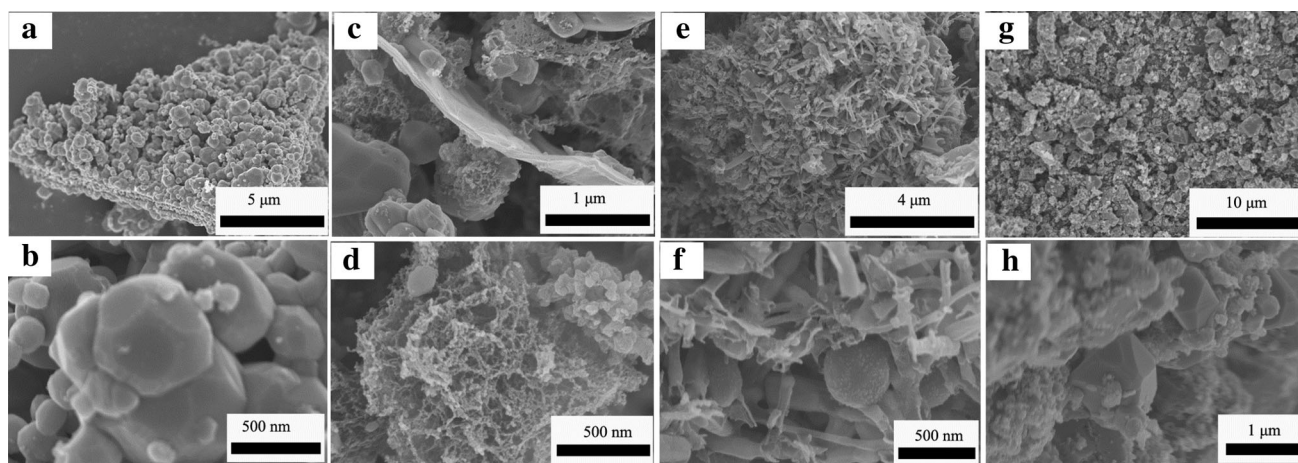


Fig. 7 SEM patterns of the GO/Ferrite composites under different solvents at GO = 0.1% (a, b water; c, d ethylene glycol; e, f ethylene glycol and glycerol; g, h glycerol)

curved graphite coating magnetic particles with rod structure. In glycerol system, the products after calcination are mainly composed by separated graphene and ferromagnetic materials. Compared with other solvents, the calcined samples in water possess high adsorption, even dispersion and controllable morphology.

Figures 8 and 9 show the SEM patterns of the roasted samples under different amounts of GO. At GO = 0.5 wt%, as it is depicted in Fig. 8a, b, ferrites are adsorbed on the graphene layer closely, in rod or hexagonal structure, with an average diameter about 180 nm and length about 1 μm. In Fig. 8c, d, with 1.0 wt% GO added,

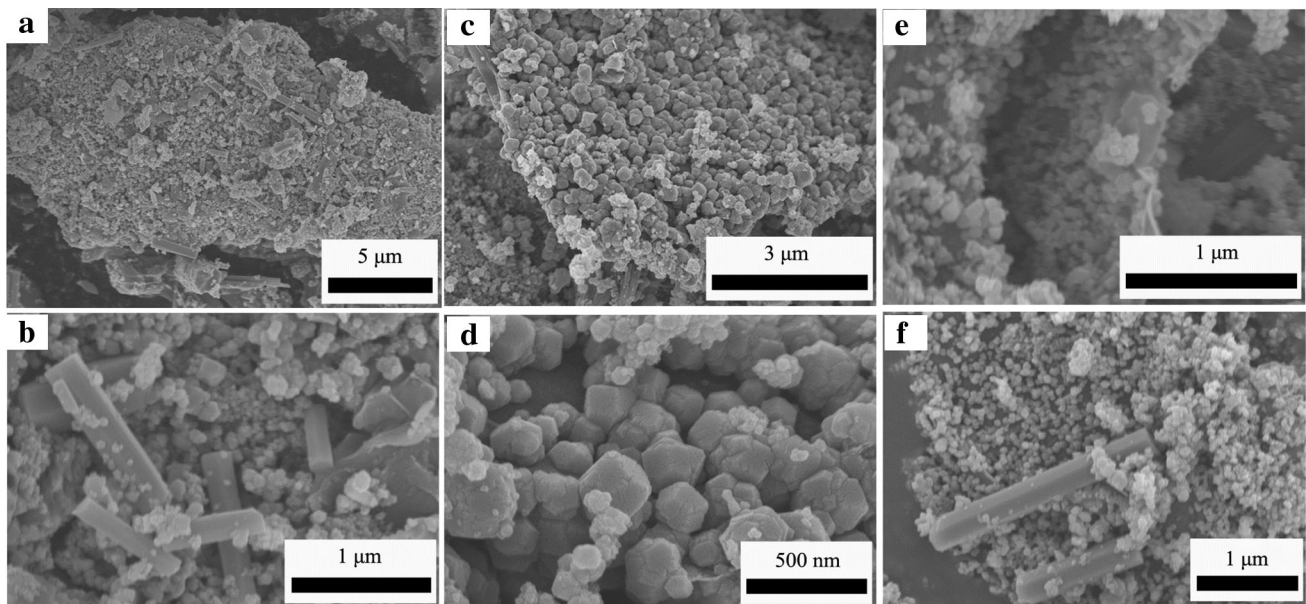


Fig. 8 The SEM figure of precursors under different GO in water system (a, b 0.5 wt%; c, d 1.0 wt%; e, f 2.0 wt%)

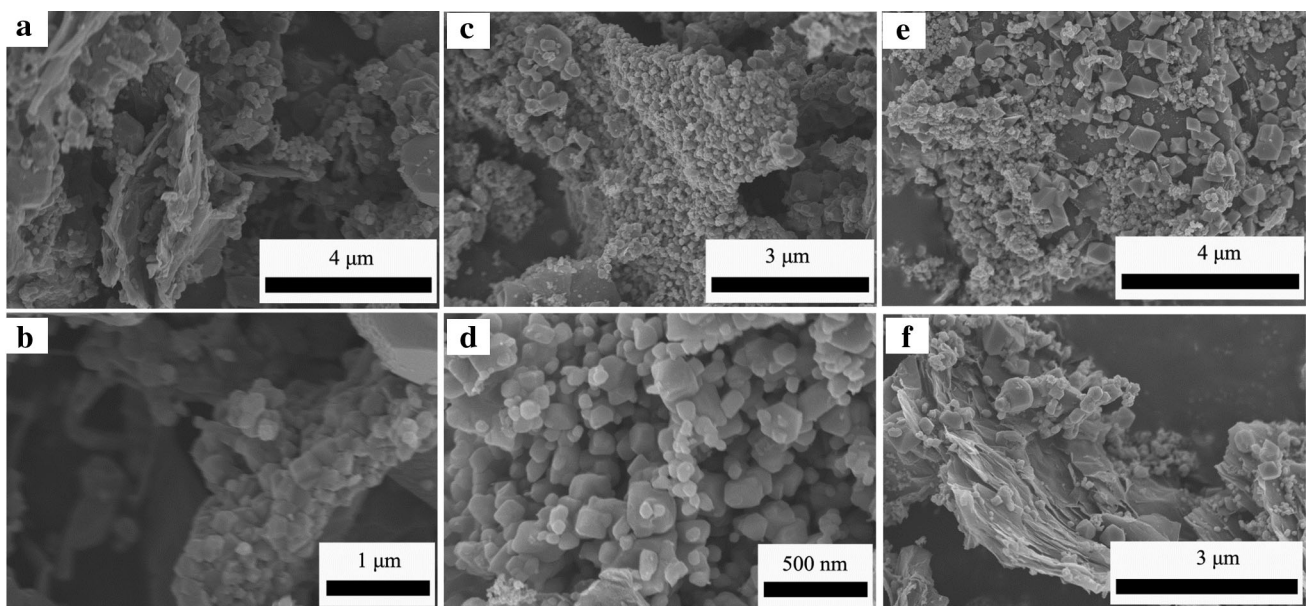


Fig. 9 SEM figures of roasted samples under different GO ratio. (a, b 0.5 wt%; c, d 1.0 wt%; e, f 2.0 wt%)

only 300 nm polyhedral nanoparticles appear with no rod structure. Along with the increase of GO, at GO = 2.0 wt%, the 50 nm diameter spherical ferrites with relatively soft distribution appear, as well as the nanorods of 400 nm diameter and 2.5 μm length. In Fig. 9a, b, with 0.5 wt% GO added, 150 nm Ferrites are embedded on the graphene sheets and covered layer by layer. With 1.0 wt% GO added, 300 nm polyhedron ferrites are absorbed on both sides of the graphene sheets. At GO = 2.0 wt%, as it is presented in Fig. 9e, f, the roasted magnetic particles on the graphene sheet are composed by 200 nm spherical

particles and 600 nm octahedral spinel ferrite, which is corresponding to the results of XRD graph.

From the SEM results, more ferrites with higher coverage on graphene appear along with the increase of GO, with its morphology changed to six prism, polyhedron or nanorods. And the ferrite transforms into Co and FeCo alloy after calcination. However, more is not the better, if the mass of GO increases blindly, ferromagnetic coverage ratio will decline gradually. Comparing the SEM results of the GO/Ferrite composites in Fig. 9 with the results in Fig. 7a, b, the optimum GO mass can be set as 0.1 wt%,

with more even distributed and better surface combining samples obtained.

3.4 The dielectric and magnetic properties of GO/Ferrites

3.4.1 Permittivity and permeability analysis

Figure 10 shows the real and imaginary parts of permittivity and permeability of the reduced graphene oxide/ferrite (RGO-FM) composites under different GO mass ratio, 0.1, 0.5, 1.0 and 2.0 wt%, respectively. At GO = 0.1 wt%, the ϵ' value at 1–12 GHz ranges from 27.22 to 28.82 and reaches 18.05 after 12 GHz, while the ϵ'' value begins about 2.72 at 2 GHz and increases continually to 13.56 at 14.20 GHz, then decreases to 10.01. At GO = 0.5 wt%, the ϵ' value ranges from 38.55 to 29.17 among 2–18 GHz, with the maximum value appearing at 13.41 GHz, while the ϵ'' value continually ranges from 6.62 to 10.58.

Overall, ϵ' value of the samples decreases with the increase of frequency, which indicates the apparent dielectric dispersion, while the ϵ'' shows a rising relaxation oscillation loss of samples for the vibrated change [36]. At GO = 1.0 wt%, ϵ' value drops from 23.39 to 17.16, but the ϵ'' first decreases and then increases, with the value ranges between 5.00 and 9.13. With GO = 2.0 wt%, the relative permittivity is the smallest among the samples, with the maximum ϵ' value of 6.60 and ϵ'' about 0.16, respectively. With the increase of GO, the value of complex permittivity first increases, then decreases and reaches the maximum value at GO = 1.0 wt%. Two reasons contribute to this phenomenon. On the one hand, according to the theory of free electrons [37],

$$\epsilon'' = \frac{1}{2\pi\epsilon_0\rho f} \quad (2)$$

the higher conductivity of GO lowers the resistivity of the material and leads to the increase of ϵ'' [38]. On the other hand, the different charge transition occurs between the

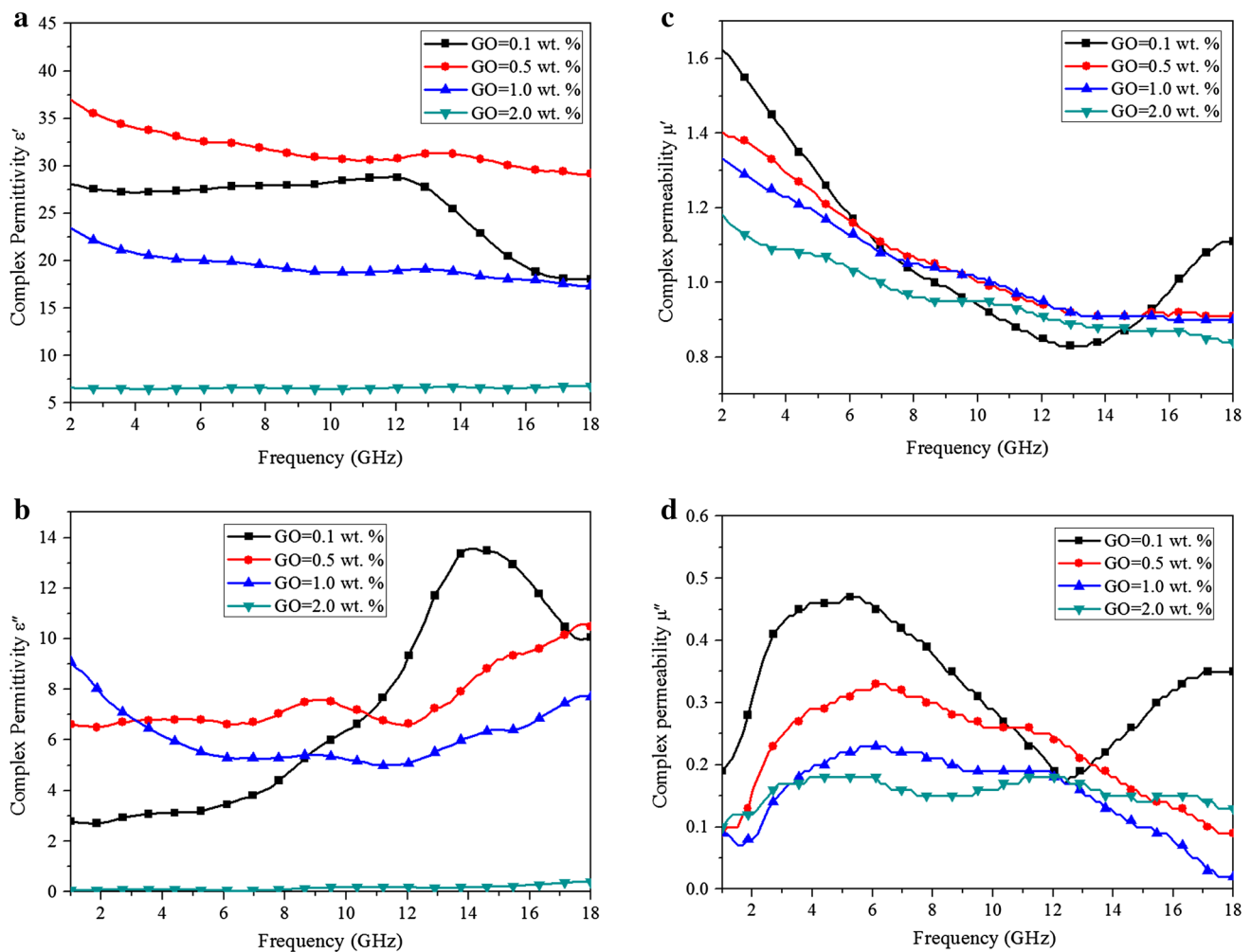


Fig. 10 Electromagnetic parameters of RGO-FM (a ϵ' ; b ϵ'' ; c μ' ; d μ'')

ferromagnetic and graphene, which may decrease the ε'' of the composites [39, 40].

At GO = 0.1 or 0.5 wt%, the surface coverage ratio of the ferromagnetic materials on graphene is higher than that of others. The electrons transformation from the surface of ferromagnetic materials to graphene results in the increase of the conductivity of graphene. The relaxation effect of dielectric dispersion and electrons movement leads to the increase of the permittivity [41]. While, along with the increase of GO, such as on the condition of GO = 1.0 or 2.0 wt%, only rough interface has been formed between the graphene and ferromagnetic materials. XRD patterns also reveal the stack problem of graphene resulting from its lower absorbing characteristic peaks. Therefore, it is difficult for graphene to transfer electrons and introduce charge carrier, which results in the lower permittivity.

Figure 10c, d shows the real and imaginary parts of permeability of RGO-FM, respectively. At GO = 0.1 wt%, the value of μ' ranges from 0.83 to 1.86, with the maximum value appearing at 13 GHz. The μ' value at GO = 0.5, 1.0 and 2.0 wt% is in accordance with 0.91–1.41, 0.90–0.90 and 0.84–1.24, respectively, which presents a reduction of the real part of permeability along with the increase of GO. It is also the same with the imaginary part of permeability. For the samples under GO = 0.1, 0.5, 1.0 and 2.0 wt%, the imaginary part of permeability ranges in 0.17–0.47, 0.09–0.33, 0.07–0.23 and 0.10–0.18, respectively. Although the ferromagnetic resonance natural peaks of the samples are apparent in 5–6 GHz, there is no apparent peak resulting from the intrinsic damping effect and interface effect in higher frequencies range (12–18 GHz) except for the samples at GO = 0.1 wt%, which proves the optimal electromagnetic match of the graphene and ferromagnetic materials [7].

Figure 11 shows the electromagnetic parameters, $\mu'' \cdot \mu'^{-2} \cdot f^{-1}$, of RGO-FM along with the increase of the frequency. It can be found that the parameter value

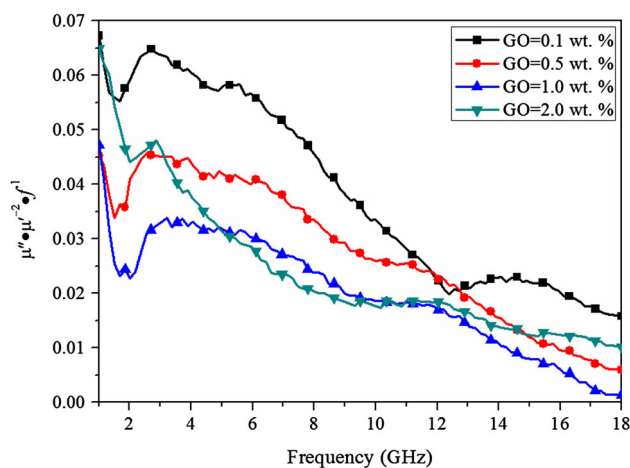


Fig. 11 The permeability of GO/ferrite composites with frequency

declines gradually with the increase of frequency, which indicates that the electromagnetic loss is not only caused by single eddy current loss, but the natural ferromagnetic resonance and the interface loss also play such an important role.

The dielectric loss tangent ($\tan \delta_e$) and magnetic loss tangent value ($\tan \delta_m$) of RGO-FM have been shown in Fig. 12. At GO = 0.1 wt%, the $\tan \delta_e$ of the samples continues to increase from lower to higher frequency, with the range from 0.10 to 0.64 and the peak appearing at 16.0 GHz. $\tan \delta_m$ ranges from 0.20 to 0.39, peaked at 6.0 and 16.0 GHz, which presents a complementary effect in the lower frequency range. At GO = 0.5 wt%, $\tan \delta_e$ of the sample rises gradually, ranging from 0.17 to 0.36, with the $\tan \delta_m$ ranging from 0.10 to 0.29, peaked at 7.0 and 11.0 GHz and showing the good complementary effect. At GO = 1.0 wt%, $\tan \delta_e$ and $\tan \delta_m$ of the samples range from 0.26–0.44 and 0.02–0.21, respectively, with a better electromagnetic matching appearing at 1–6 and 12–18 GHz, which is consistent with the results of the Co3Fe7@C core-shell nanocomposites [42, 43]. Also, the magnetic loss is lower than that of the electric loss. In conformity with the results of permittivity, $\tan \delta_e$ and $\tan \delta_m$ rise slowly at GO = 2.0 wt%, with the range being 0.008–0.06 and 0.08–0.20, respectively. Eventually, the better absorbing intensity of absorbers in lower frequency can be achieved from the higher $\tan \delta_e$ and $\tan \delta_m$ at GO = 0.1 wt%. Also, at GO = 0.5 or 1.0 wt%, a more broadband absorption of the samples can be achieved from the complementary effect of magnetic and electric loss in 1–18 GHz.

3.4.2 Absorbing performance analysis

According to transmission line theory, electromagnetic parameters of the materials are calculated and presented in Fig. 13a–d at GO = 0.1, 0.5, 1.0 and 2.0 wt%, respectively.

From Fig. 13a, it can be found that, at GO = 0.1 wt%, the reflectivity of the sample can reach -9.19 dB at 9.0 GHz of 2 mm thickness, with the bandwidth below -5 dB reaching 5.4 GHz (6.7–12.1 GHz). With the increase of thickness, the corresponding frequencies of the maximum absorption transform to lower frequency range and constantly improve the reflectivity peak, 3 mm with the reflectivity peak of -15.26 dB at 3.9 GHz, 3.5 mm corresponding to -17.15 dB with the frequency below -10 dB being 2.8–3.8 GHz, 5 mm thickness at 2.18 GHz with the strongest reflection peak of -25.60 dB. When GO are increased to 0.5 wt%, the sample of 2 mm thickness can reach the reflectivity peak of -9.27 dB at 8.48 GHz, with the bandwidth below -5 dB about 4.6 GHz (6.4–11.0 GHz). At 3 mm thickness, the reflectivity peak appears at 3.6 GHz being -12.78 dB, 3.5 mm

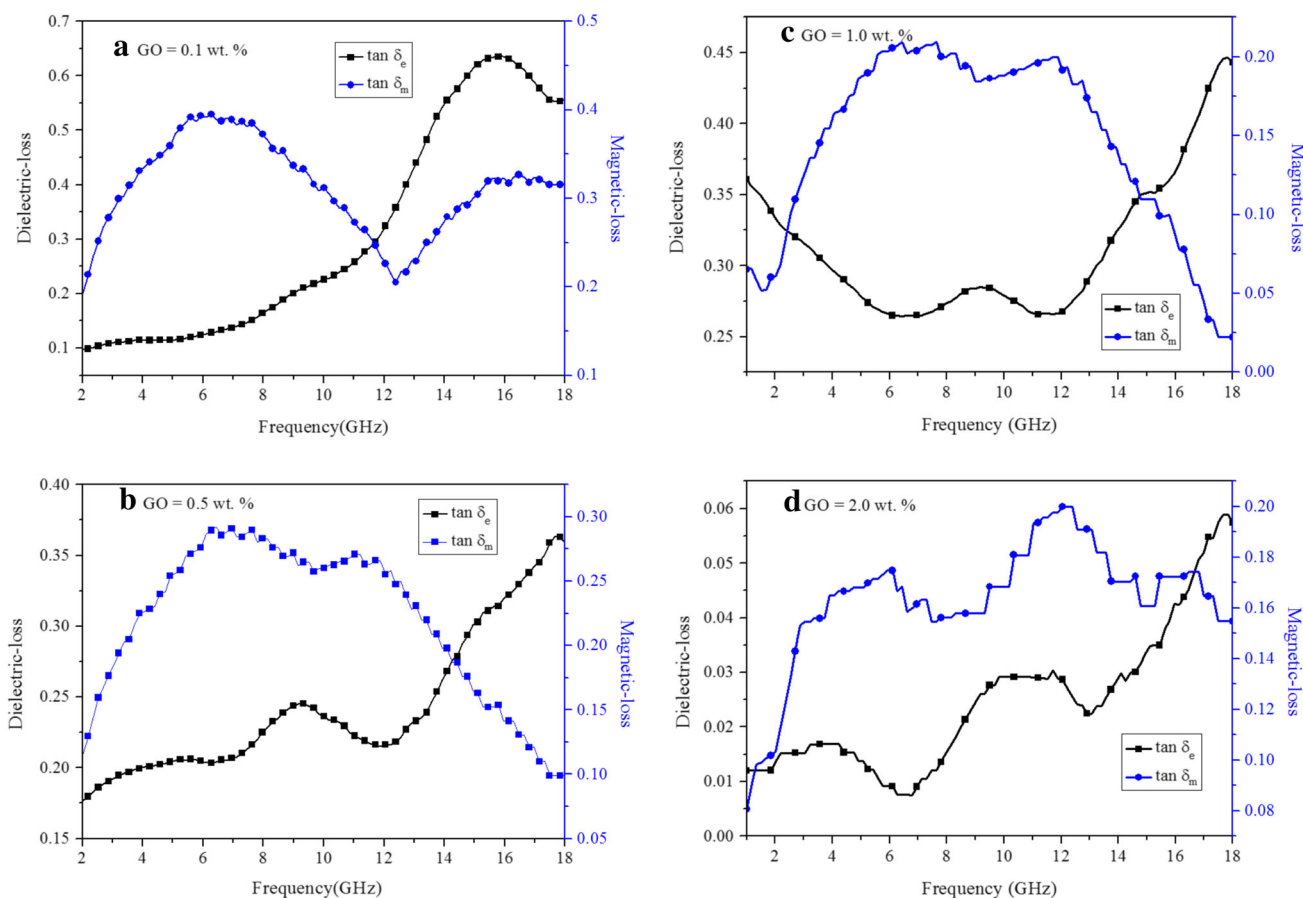


Fig. 12 The loss tangent of GO/ferromagnetic (**a** GO = 0.1 wt%; **b** GO = 0.5 wt%; **c** GO = 1.0 wt%; **d** GO = 2.0 wt%)

corresponding to -14.25 dB at 3.0 GHz. Comparatively, the strongest reflection peak appears at 1.7 GHz of -18.80 dB under 6 mm thickness.

At GO = 0.5 wt%, the reflection loss of the sample is slightly lower than that of GO = 0.1 wt%, which is in conformity with the loss tangent analysis. At 1 mm thickness and GO = 0.5 wt%, the reflectivity below -5 dB ranges from 10.9 to 17.7 GHz with the bandwidth about 6.8 GHz, which indicates the superior RL property of the samples in higher frequency at GO = 0.1 wt%. The results are attributed to the complementary effect of electric and magnetic loss at GO = 0.5 wt%. At GO = 1.0 wt%, the reflectivity peak of the samples at 1.5 mm thickness reaches -13.27 dB at 11.6 GHz, with the bandwidth below -10 dB being about 2.6 GHz (10.3–12.9 GHz). At 2 mm thickness, the RL peak about -13.29 dB appears at 8.3 GHz, with the bandwidth below -10 dB being 2.1 GHz (7.3–9.4 GHz). With the increase of thickness, the maximum absorption frequencies are transformed to the lower frequency range, with a constantly improved reflectivity peak. 3.5 mm thickness corresponds to twin peaks at 4.3 GHz and 15.6 GHz, respectively, with the strongest reflection peak appearing at 6 mm and

reaching -16.09 dB at 2.3 GHz. Due to the complementary property of the dielectric and magnetic loss of the composites, the increase of the GO largely broadens the wide absorption bandwidth, but lowers the value of the reflectivity peak. As it is shown in Fig. 13d, three reflectivity tips of the samples of 6 mm thickness appear at S and Ku bands. When the thickness is changed to 10 mm, the reflectivity appears at S, X and Ku bands with both of the two peaks below -10 dB at 9.0 and 15.4 GHz. Compared with the electromagnetic parameters and RL results of the single ferrites mentioned in our previous work [42], it indicates that the graphene oxides originated from the roasting process promote the increase of conductivity and permittivity of the composites effectively and achieve a better microwave absorbing property, especially for the lower frequency range.

4 Conclusions

The graphene-based composites have been designed and prepared successfully by hydrothermal and calcination process. The effect of the solvent and the mass ratio of GO

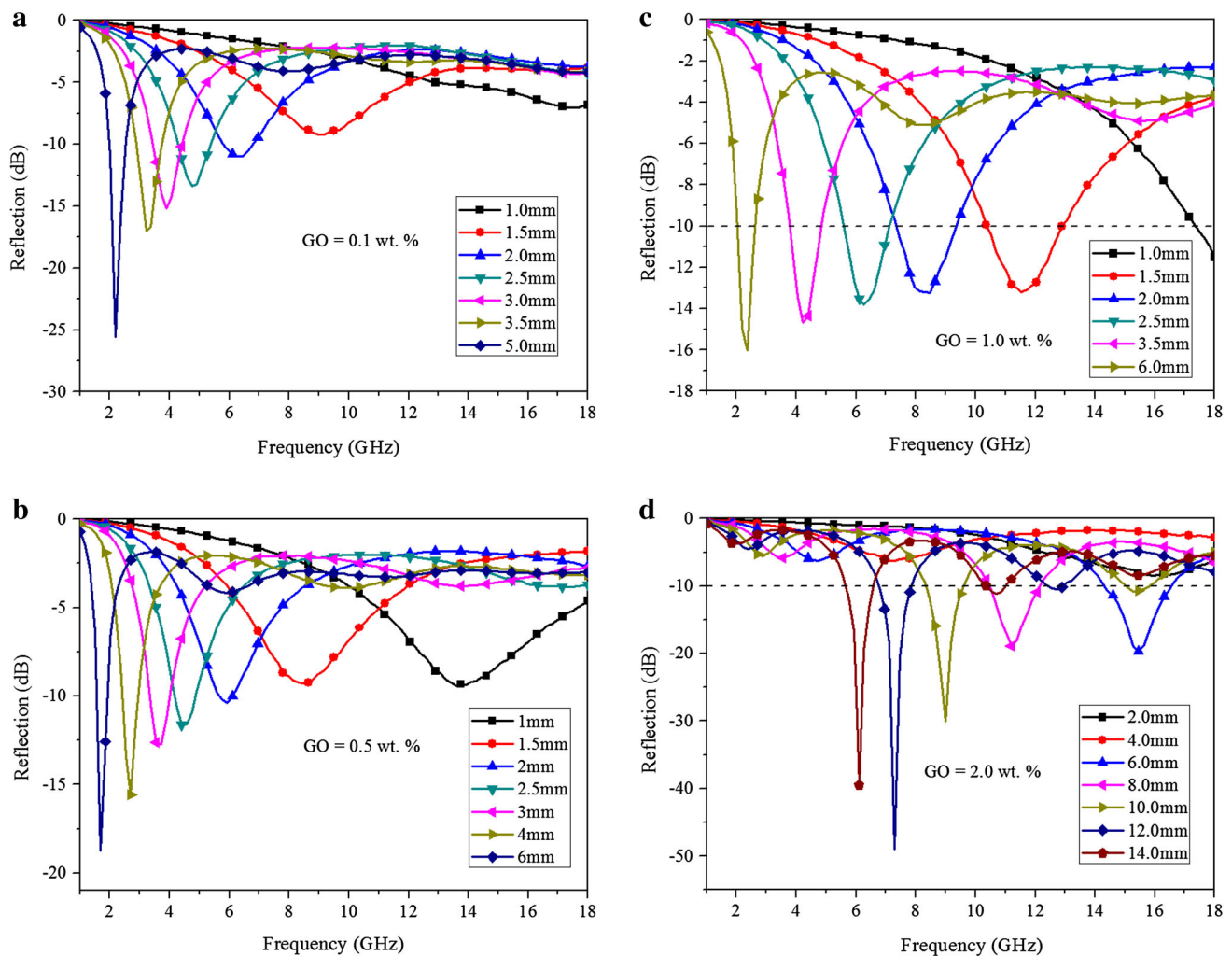


Fig. 13 The reflectivity loss of GO/ferrites at different dosage of GO (a GO = 0.1 wt%; b GO = 0.5 wt%; c GO = 1.0 wt%; d GO = 2.0 wt%)

on the morphology of the target samples has been analyzed. The results show that the solvent has a great effect on the crystallization and morphology of the samples, while the dosage of GO greatly affects the coverage of the magnetic ferrites and their morphology. Comparatively, the samples under water can get the evenly distributed polyhedral ferrites on the graphene sheets, with high coverage ratio and no aggregation. Along with the increase of GO, ferrites of lower coverage on graphene appear, with its morphology changed to six prism, polyhedron or nanorods, and the ferrite transforming into Co and FeCo alloy after calcination. Given this, the optimal samples have been designed and prepared at GO = 0.1 wt% under water system. The electromagnetic parameters and microwave absorbing properties of composites have been measured and analyzed. The results reveal that the addition of GO improves the absorbing properties of ferrite nanoparticles, which promotes a stronger RL peak in lower frequency

range. At GO = 0.1 wt%, the RL peak appears at 3.3 GHz up to -17.15 dB under 3 mm thickness, with the bandwidth below -10 dB ranging from 2.8 to 3.8 GHz. For GO = 1.0 wt%, the bandwidth below -10 dB reaches about 2.6 GHz (10.3–12.9 GHz) at 1.5 mm thickness, with the RL peak up to -13.27 dB at 11.6 GHz. The twin peaks appear at 4.3 and 15.6 GHz of 3.5 mm thickness, respectively.

Acknowledgements We gratefully acknowledge the School of Mechatronical Engineering, Beijing Institute of Technology for financial support of this project.

References

1. M. Peplow, Nat. News. (2006). doi:10.1038/news060320-6
2. T. Auld, M.P. McHenry, J. Whale, Renew. Energy **55**, 24 (2013)
3. D. Schurig, J.J. Mock, B.J. Justice, S.A. Cummer, J.B. Pendry, A.F. Starr, D.R. Smith, Science **314**, 977 (2006)

4. X.H. Gong, H.Y. Tan, H.D. Meng, J.M. Guo, *Signal Proc.* **100**, 186 (2014)
5. A. Wise, M. Tur, A. Zadok, *Opt. Express* **19**, 21945 (2011)
6. Z.G. Sun, X.J. Qiao, X. Wan, Q.G. Ren, W.C. Li, S.Z. Zhang, X.D. Guo, *Appl. Phys. A* **122**, 87 (2016)
7. T. Wang, H.D. Wang, X. Chi, R. Li, J.B. Wang, *Carbon* **74**, 312 (2014)
8. C. Lee, X.D. Wei, J.W. Kysar, J. Hone, *Science* **321**, 385 (2008)
9. M.J. Allen, V.C. Tung, R.B. Kaner, *Chem. Rev.* **110**, 132 (2010)
10. F. Schedin, A.K. Geim, S.V. Morozov, E.W. Hill, P. Blake, M.I. Katsnelson, K.S. Novoselov, *Nat. Mater.* **6**, 652 (2007)
11. P. Bhattacharya, C.K. Das, *J. Mater. Sci-Mater. El.* **24**, 1927 (2013)
12. Y.N. Tang, Z.Y. Liu, Z.G. Shen, W.G. Chen, D.W. Ma, X.Q. Dai, *Sens. Actuators B* **238**, 182 (2017)
13. M.F. El-Kady, V. Strong, S. Dubin, R.B. Kaner, *Science* **335**, 1326 (2012)
14. H. Zhang, X.J. Lv, Y.M. Li, Y. Wang, J.H. Li, *ACS Nano* **4**, 380 (2010)
15. Q. Wan, M.Y. Liu, Y.L. Xie, J.W. Tian, Q. Huang, F.J. Deng, L.C. Mao, Q.S. Zhang, X.Y. Zhang, Y. Wei, *J. Mater. Sci.* **52**, 504 (2017)
16. A.K. Geim, K.S. Novoselov, *Nat. Mater.* **6**, 183 (2007)
17. D. Kuang, W.B. Hu, *J. Inorg. Mater.* **28**, 235 (2013)
18. X.Y. Wu, S.M. Li, J.H. Liu, M. Yu, B. Wang, *J. Inorg. Mater.* **29**, 845 (2014)
19. X. Huang, X.Y. Qi, F. Boey, H. Zhang, *Chem. Soc. Rev.* **41**, 666 (2012)
20. H.M.A. Hassan, V. Abdelsayed, A.E.R.S. Khder, K.M. Abou-Zeid, J. Turner, M.S. El-Shall, S.I. Al-Resayes, A.A. El-Azhary, *J. Mater. Chem.* **19**, 3832 (2009)
21. D.P. Sun, Q. Zou, G.Q. Qian, C. Sun, W. Jiang, F.S. Li, *Acta Mater.* **61**, 5829 (2013)
22. S. Ameer, I.H. Gul, M. Mujahid, *J. Alloy. Compd.* **642**, 78 (2015)
23. Y. Wang, W.Z. Zhang, C.Y. Luo, X.M. Wu, Q.G. Wang, W.X. Chen, J.H. Li, *Ceram. Int.* **42**, 17374 (2016)
24. Y. Wang, X.M. Wu, W.Z. Zhang, S. Huang, *J. Magn. Magn. Mater.* **404**, 58 (2016)
25. H.P. Cong, J.J. He, Y. Lu, S.H. Yu, *Small* **6**, 169 (2010)
26. N. Tombros, A. Veligura, J. Junesch, M.H.D. Guimaraes, I.J. Vera-Marun, H.T. Jonkman, B.J. van Wees, *Nat. Phys.* **7**, 697 (2011)
27. H.L. Xu, H. Bi, R.B. Yang, *J. Appl. Phys.* **111**, 552 (2012)
28. W.C. Li, X.J. Qiao, Q.Y. Zheng, T.L. Zhang, *J. Alloy. Compd.* **509**, 6206 (2011)
29. V.K. Singh, A. Shukla, M.K. Patra, L. Saini, R.K. Jani, S.R. Vadera, N. Kumar, *Carbon* **50**, 2202 (2012)
30. S. Afghahi, A. Shokuhfar, *J. Magn. Magn. Mater.* **370**, 37 (2014)
31. D.C. Marcano, D.V. Kosynkin, J.M. Berlin, A. Sinitskii, Z.Z. Sun, A. Slesarev, L.B. Alemany, W. Lu, J.M. Tour, *ACS Nano* **4**, 4806 (2010)
32. S.F. Pei, H.M. Cheng, *Carbon* **50**, 3210 (2012)
33. X.C. Zhao, Z.M. Zhang, L.Y. Wang, K. Xi, Q.Q. Cao, D.H. Wang, Y. Yang, Y.W. Du, *Sci. Rep.* **3**, 3421 (2013)
34. D. Hisada, Y. Fujiwara, H. Sato, M. Jimbo, T. Kobayashi, K. Hata, *J. Magn. Magn. Mater.* **323**, 3184 (2011)
35. J.C. Meyer, A.K. Geim, M.I. Katsnelson, K.S. Novoselov, T.J. Booth, S. Roth, *Nature* **446**, 60 (2007)
36. X.G. Liu, Z.Q. Ou, D.Y. Geng, Z. Han, J.J. Jiang, W. Liu, Z.D. Zhang, *Carbon* **48**, 891 (2010)
37. R. Simon, R.W. John, V.D. Theodore, *Int. J. Electron.* **21**, 6 (1966)
38. C. Wang, X.J. Han, P. Xu, X.L. Zhang, Y.C. Du, S.R. Hu, J.Y. Wang, X.H. Wang, *Appl. Phys. Lett.* **98**, 7 (2011)
39. G. Giovannetti, P.A. Khomyakov, G. Brocks, V.M. Karpan, J. van den Brink, P.J. Kelly, *Phys. Rev. Lett.* **101**, 026803 (2008)
40. K. Pi, K.M. McCreary, W. Bao, W. Han, Y.F. Chiang, Y. Li, S.W. Tsai, C.N. Lau, R.K. Kawakami, *Phys. Rev. B* **80**, 7 (2009)
41. T. Sameshima, H. Hayasaka, T. Haba, *Jpn. J. Appl. Phys.* **48**, 2 (2009)
42. X.D. Guo, X.J. Qiao, Q.G. Ren, X. Wan, W.C. Li, Z.G. Sun, *Appl. Phys. A* **120**, 43 (2015)
43. R.C. Che, L.M. Peng, X.F. Duan, Q. Chen, X.L. Liang, *Adv. Mater.* **16**, 401 (2004)